Environmental Science
Water Research & Technology

ROYAL SOCIETY OF CHEMISTRY

PAPER

View Article Online
View Journal

Cite this: DOI: 10.1039/d5ew01131k

Suspect screening of disinfection byproduct precursors in water treatment processes using ultrahigh resolution mass spectrometry

Juliana R. Laszakovits *[ab] and Allison A. MacKay[a]

Disinfection byproducts (DBPs) formed by reaction between dissolved organic matter (DOM) and chlorine remain a persistent challenge for producing high quality drinking water. The complex chemical mixture of DOM has hindered the development of targeted removal strategies for DBP precursors. Here, we used ultrahigh resolution mass spectrometry to investigate how the formation of DBPs from components of three different DOM isolates (terrestrial, wastewater effluent-derived, and algal-impacted) responded to conventional treatments of permanganate oxidation, alum coagulation, and activated carbon sorption. We report that the three isolates responded differently to permanganate oxidation, a conventional strategy to remove DBP precursors, in terms of both carbonaceous and nitrogenous DBP formation potential. In some cases, permanganate could directly oxidize DBP precursors or improve the removal of DBP precursors by subsequent alum coagulation; while in other cases, permanganate oxidation was not effective. Combinations of activated carbon sorption and alum coagulation were widely effective in reducing DBP formation from all isolates studied, but the removed precursors differed between isolates. Finally, possible persistent DBP precursors, not removed by any treatment, were identified with plausible chemical structures proposed based on the ionization techniques and ion types. Overall, the identification of DBP precursors can aid in the development of targeted removal strategies.

Received 16th November 2025,
Accepted 18th May 2026

DOI: 10.1039/d5ew01131k

rsc.li/es-water

Water impact

Disinfection byproducts (DBPs) formed during drinking water treatment by reaction between chlorine and natural organic matter have been an ongoing challenge for utilities. Here, we provide fundamental insight into chlorination reaction with natural organic matter, leading to the identification of suspect DBP precursor formulas.

Introduction

Disinfection byproducts (DBPs) are formed during drinking water treatment when disinfectants, including chloramine and chlorine, react with dissolved organic matter (DOM).[1,2] Many DBPs are known or suspected carcinogens which pose public health concerns.[2–4] In the United States, two classes of carbonaceous-DBPs (C-DBPs) are regulated by the United States Environmental Protection Agency (EPA): trihalomethanes (THMs, 80 ppb) and haloacetic acids (HAAs, 60 ppb).[1,2,5] Models exist that can predict the formation of regulated C-DBPs reasonably well for a given source water using total dissolved organic carbon (DOC) concentration and specific ultraviolet absorbance at 254 nm (SUVA-254).[6,7] Studies of model compounds suggest that activated phenols are the likely precursors for THMs and HAAs and they are known to be abundant in terrestrial-derived DOM.[1,8] Although there is strong evidence that activated phenols are responsible for the formation of C-DBPs, current treatment practices do not specifically target these moieties nor other lesser-known key DOM compounds that react with chlorine.[1]

The management of nitrogenous DBPs (N-DBPs) is a greater challenge for drinking water plant operators.[9] Toxicology studies suggest that N-DBPs are more toxic compared to regulated C-DBPs.[10] Important N-DBP classes include haloacetonitriles, halonitromethanes (such as chloropicrin), and nitrosamines.[9] These compounds are formed in greater abundance when chloramine disinfectants are used.[9,11] However, they can also be formed through chlorine reaction with organic nitrogen constituents in DOM.[9,12] Organic nitrogen compounds are generally more

[a] Department of Civil, Environmental, and Geodetic Engineering, The Ohio State University, Columbus, OH, 43210, USA
[b] Department of Environmental Systems Science, Institute of Biogeochemistry and Pollutant Dynamics, ETH-Zuerich, Zuerich, 8002, Switzerland.
E-mail: jlaszakovits@ethz.ch

abundant in microbial DOM than terrestrial DOM.[12] Microbial DOM dominates in water sources that are drought-impacted and contain high levels of wastewater effluent DOM, in water reuse scenarios, and waters that are impacted by algal blooms.[1,12] While our knowledge of the processes that lead to N-DBP formation continues to expand, specific precursors of these DBPs have not been identified and therefore, are unable to be targeted by treatment practices.

Currently, in the absence of known DOM component precursors, DBP management employs a blanket approach. Most DBP management focuses on removing as much DOM as possible, with a particular focus on aromatic moieties.[6] Removal approaches include alum coagulation and activated carbon sorption.[13–18] Yet, in some cases, the application of these approaches can increase the formation of certain DBPs.[19–22] For example, it has been observed repeatedly that granular activated carbon treatment can result in an increase in DBP formation.[19–22] This outcome is believed to occur by preferential bulk removal of certain components that shift disinfectant reactivity toward a different subset of DOM precursor components, but the molecular reasons remain unknown.[19–22] Another strategy is to oxidize DOM with ozone or permanganate to pre-emptively reduce DOM component reactivity in subsequent disinfectant treatment. Permanganate oxidation is widely believed to remove DBP precursors.[23–27] However, previous work on the impact of permanganate oxidation on DBP formation used dosing levels of permanganate that exceed realistic drinking water practices, nor have previous studies considered coupled treatment operations, such as coagulation and activated carbon.[23–25] Thus, the impact of permanganate oxidation on DBP formation remains uncertain.

Previous work from our group suggested that permanganate oxidation has potential to decrease the formation of C-DBPs from both terrestrial and microbial sources of DOM in conventional water treatment.[28,29] We used ultrahigh-resolution mass spectrometry to show that coagulation tended to remove high molecular weight, aromatic DOM components from Suwannee River Fulvic Acid (SRFA), a terrestrial-derived DOM isolate.[29] This outcome suggests there could be a reduction in subsequent THM and HAA formation. Activated carbon sorption, in contrast, removed lower molecular weight aliphatic fractions.[29] Thus, the activated carbon treatment impact on DBP formation was unclear.[29] Pre-treatment of samples with permanganate oxidation improved the removal of DOM by coagulation through the oxidation of aromatic components.[29] This observation suggests permanganate could reduce DBP formation through improved DOM removal by coagulation. Thus, the molecular level trends observed for SRFA fit well with the conceptual model of DBP formation from literature studies.

Trends in molecular level changes of microbial DOM isolates in conventional treatments differed from literature expectations. The microbial-derived DOM isolates contained components that were more homogeneous and dominated by peptides and lipid-like components, with fewer aromatic components than for SRFA.[29] The DOM removal efficacy by both alum coagulation and activated carbon was similar, regardless of the order applied, and thus suggests that DBP formation could be similarly reduced in an additive way.[29] Pre-treatment of microbial DOM by permanganate resulted in oxidation of nitrogenous and aliphatic DOM components that are less studied with respect to DBP formation. Overall, the variation in ways that different DOM isolates responded to treatment, particularly permanganate pre-oxidation, warrants investigation into the effects of DOM component alterations on DBP formation.

Here, we address the interplay between DOM molecular level changes and subsequent DBP formation during typical drinking water treatment operations for three different DOM isolates – terrestrial (SRFA), wastewater effluent-derived (EfOM), and algal-derived (AOM) – using ultrahigh resolution-mass spectrometry. We investigated how the commonly applied treatments of permanganate oxidation, alum coagulation, and activated carbon sorption impacted DBP formation potential. THMs, HAAs, and N-DBPs were monitored in aliquots removed for chlorination, before and after, each treatment step to examine sequential changes in DBP formation potential. We defined suspect DBP precursors as DOM components that were no longer observable in a sample ultra-high resolution-mass spectrum after that sample had undergone chlorination. We used these presence/absence comparisons of mass spectra to examine the impact of permanganate treatment on DBP formation, to gain insight into suspect N-DBP precursors, and to understand how shifts in DOM component distributions following treatment may also be associated with suspect DBP precursor removal. We then leveraged the ion formation patterns of these suspected precursor formulas to propose chemical structures for the DOM components most persistent across the applied water treatments.

Materials & methods

Suwannee River Fulvic Acid (SRFA) was purchased from the International Humic Substances Society. Algal-impacted organic matter was isolated from water collected from Grand Lake St. Mary's reservoir (Celina, OH, USA) in October 2018. The algal-impacted water sample was filtered using 0.45 μm glass fibre filters and the algal organic matter (AOM) isolate was obtained using Agilent Bond Elut Priority Pollutant (PPL) cartridges as described by Dittmar *et al.*[30] The wastewater effluent organic matter isolate (EfOM) was obtained using the same method as for the AOM isolate after collecting water from Jackson Pike wastewater treatment plant (Columbus, OH, USA) in July 2019. Optima mass spectrometry grade methanol (Fisher) was used in the DOM extractions. A stock alum solution was prepared using aluminium sulphate hydrate (97+%, Alfa Aesar) at a concentration of 50 g L^{-1} as alum. A stock potassium permanganate solution (0.8 g L^{-1}) was prepared from solid potassium permanganate ($KMnO_4$,

>99%, Acros Organics). Calgon Norit powdered activated carbon (PAC) from bituminous coal was sieved to remove particles larger than 45 μm, washed to remove fines using a 0.45 μm polyvinylidene fluoride (PVDF) filter, and dried at 100 °C for at least 48 hours, before preparing a stock solution at 10 g L^{-1} in high purity water. The following salts were used to prepare model water solutions that varied slightly for each DOM isolate so that solution pH values were realistic for waters dominated by the respective DOM source types: sodium bicarbonate (Fisher, certified American chemical society (ACS) grade), calcium chloride dihydrate (Fisher, certified ACS), calcium sulphate dihydrate (Sigma Aldrich, ACS reagent grade), magnesium sulphate heptahydrate (Sigma Aldrich, ACS reagent grade), potassium chloride (Fisher, certified ACS), ammonium nitrate (Sigma-Aldrich, ACS reagent, ≥98%), ferric chloride anhydrous (Fisher, laboratory grade), sodium dibasic phosphate anhydrous (Fisher, ≥99%), and potassium carbonate (Fisher, reagent grade). The pH values and cation and anion concentrations for each model water background are summarized in Table S1. Sodium hypochlorite (11–15% available chlorine) was purchased from Alfa Aesar. Trimethoxybenzene (Sigma-Aldrich, ≥99%) was prepared in aqueous solution at a concentration of 3 mM using high purity water. Optima MS grade methanol (Fisher), stabilized methylene chloride (Fisher, certified ACS), and methyl *tert*-butyl ether (MTBE, Alfa Aesar. High performance liquid chromatography (HPLC) grade) were used for solid phase extraction procedures. Sodium phosphate dibasic heptahydrate (Fisher, certified ACS) and sodium phosphate monobasic monohydrate (Fisher, certified ACS) were used to prepare a 1 M pH 7 phosphate buffer (for chlorination) and a 1 M pH 4.8 phosphate buffer (for volatile DBP extraction).

Three main treatment trains were simulated so that the treatments were applied in a realistic order while also isolating the effect of the individual treatments on DOM composition: permanganate oxidation, alum coagulation, and activated carbon sorption (Fig. 1). Each DOM isolate was investigated separately using an initial concentration of 10 mg_C L^{-1}. Permanganate pre-oxidation was applied at 1 mg L^{-1} $KMnO_4$ and reacted overnight prior to coagulation. Permanganate pre-oxidation was followed by coagulation using 50 mg L^{-1} of alum (2 minutes rapid mix, 30 minutes slow mix, and allowed to settle for at least 4 hours). Finally, clarified water was removed and activated carbon sorption was applied using a concentration of 25 mg L^{-1} PAC with a 2-hour contact time and removal of PAC by filtration using 0.45 μm PVDF (Fig. 1A).[31] The latter PAC application was used to simulate granular activated carbon. We note that this could lead to differences between simulated and real treatments, but prior work has shown that granular activated carbon and PAC remove similar DOM components.[32,33] Thus, the types of components that were removed by our post-coagulation PAC treatment will be comparable to those removed by granular activated carbon. The second treatment sequence involved the application of coagulation directly followed by activated carbon sorption, again to simulate granular activated carbon (Fig. 1B). In the third treatment sequence applied, PAC was applied prior to coagulation, which is a typical order for PAC treatment (Fig. 1C). The chemical dosages and contact times used were the same for each treatment application, regardless of sequence. Following each treatment step for a given treatment sequence, samples were collected for bulk property analyses, molecular level analyses (black stars), and chlorination (blue stars) (Fig. 1).

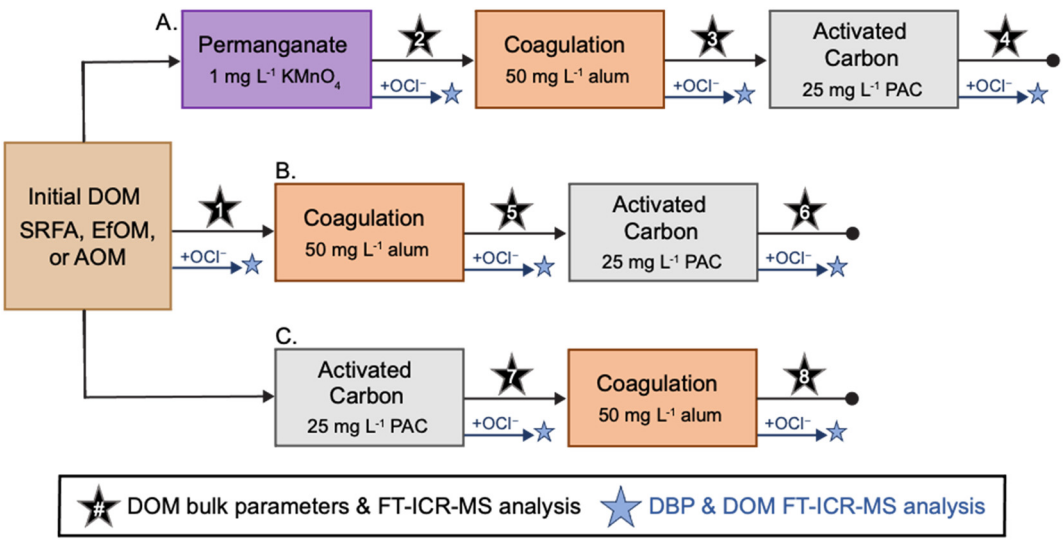

Fig. 1 Overview of experimental design. Three different organic matter isolates were used (SRFA, EfOM, and AOM) and subjected to three different treatment sequences: A. permanganate pre-oxidation followed by alum coagulation and then activated carbon sorption, B. alum coagulation followed by activated carbon sorption, and C. powdered activated carbon pre-treatment followed by alum coagulation. Black stars show where samples were analyzed for molecular composition and bulk parameters; blue stars indicate when samples were chlorinated to assess DBP formation potential and characterize molecular level changes.

Formation potential after each treatment was assessed for all samples. The stock concentration of free chlorine (as OCl^-) was measured spectrophotometrically at 292 nm (extinction coefficient of 362 M^{-1} cm^{-1}) on the day of addition.[34,35] All samples were pH adjusted to 7 using a 1 M phosphate buffer prior to chlorination. Chlorine was added to each sample (initial and 7 treated samples for each DOM isolate, blue stars in Fig. 1) at a concentration of 13 mg Cl_2 L^{-1}. The same concentration was applied for every sample to minimize chlorine residual and thereby reduce the amount of chlorine quencher required. We also note that this chlorine concentration is higher than that which is typically applied in drinking water to account for the higher DOC concentrations in the samples (10 mg_C L^{-1} compared to <2 mg_C L^{-1}). Trimethoxybenzene (15 μM) was used to quench chlorine after 48 hours of reaction. Trimethoxybenzene was chosen because most DBPs are stable in its presence, compared to other common quenchers, such as thiosulfate.[36] Typically, trimethoxybenzene is dissolved in methanol, however, during preliminary experiments, it was found that the addition of methanol greatly decreased the solid phase extraction efficiency for the DOM isolates obtained following chlorination.

Bulk DOM characterization (DOC, total dissolved nitrogen (TDN), ultraviolet-visible (UV-vis) spectroscopy, E2/E3 ratio, and SUVA-254) was conducted and described in detail in Text S1. E2/E3 (A_{250}/A_{365}) ratios were used to monitor approximate changes to DOM electron donating capacity through the postulated inverse correlation between these two properties; SUVA-254 values were used to estimate changes to DOM aromaticity through the postulated direct correlation between these two properties.[37–39] DOM was isolated after each treatment using solid phase extraction as described above.[30] Fourier transform-ion cyclotron resonance-mass spectrometry (FT-ICR-MS) analyses were conducted to characterize isolated DOM molecular level changes following methods described in Text S2. SRFA was analysed using both negative and positive mode electrospray ionization (ESI) and both negative and positive mode laser desorption/ionization (LDI); EfOM was analysed using both negative and positive mode ESI and positive mode LDI; AOM was analysed using both negative and positive mode ESI. EfOM could not be ionized using negative mode LDI; AOM was unable to be ionized by LDI due to its low abundance of aromatic compounds. We note that FT-ICR-MS is not a quantitative technique so we could only monitor changes resulting from complete component removal, which could also be indicative of ion suppression. Thus, our analysis underestimates partial removal of chemical components.

DBPs were quantified based on established EPA methods. HAAs were quantified using EPA method 557 adapted for an Exion LC and Sciex 3500 mass spectrometer.[40] Briefly, a 10 mL aliquot of solution was acidified using concentrated sulphuric acid (5%) and a ^{13}C bromoacetic acid internal standard was added at 40 ppb. Volatile C-DBPs and N-DBPs were quantified using EPA method 551 adapted to an Agilent gas chromatograph-mass spectrometer (GC-MS).[41] An extraction surrogate (1,2-dibromopropane) was added to 50 mL of chlorinated water samples before extraction into 3 mL of methyl tertbutyl ether (MTBE). This method quantified haloalkanes, haloketones, THMs, chloropicrin, and halonitriles but only trihalomethanes, haloketones, halonitriles, and chloropicrin were detected in our dataset so all data shown is for these classes. Nitrosamines were quantified by concentration using solid phase extraction according to EPA method 521 and analysed by liquid chromatography-mass spectrometry (LC-MS).[42,43] Full analytical details on DBP quantification are provided in Text S3.

This data was analysed to assess the impact of treatment steps on DBP formation, identify bulk DOM properties that drive DBP formation, and investigate molecular level changes to DOM induced by chlorination. Two main data strategies were applied in this work. First, bulk DOM properties were related to DBP formation. A stepwise linear regression was used to identify which bulk properties (DOC, TDN, SUVA-254, and E2/E3 ratio) correlated with DBP formation for each of the four classes of DBPs measured (HAAs, volatile C-DBPs, volatile N-DBPs, and nitrosamines). Interaction terms between the measured bulk properties were also considered to understand if there were joint effects that could not be ascribed to one parameter alone.

Second, chemical formulae determined by FT-ICR-MS were used to interpret changes in DBP formation induced by permanganate oxidation, to identify the most effective treatment sequences for each organic matter type, and subsequently, to identify suspect DBP precursors. DOM components were compared between mass spectra for each sample, obtained before and after chlorination of the sample. We defined suspect DBP precursors as DOM components that were no longer observable in the FT-ICR-MS spectrum of a sample after it had been chlorinated because they reacted fully with chlorine. We then tracked these from the original DOM sample through subsequent treatment steps. The DBP precursors that were removed across the treatment sequence that showed the greatest overall reduction in total DBP formation were classified as suspect precursors for C-DBPs and N-DBPs that were removed by treatment. DOM components that were present in all samples (initial and all treatments) were identified as persistent suspect DBP precursors (*i.e.*, not removed by treatment).

Results & discussion

Observed trends are broadly consistent with wider literature

We first considered how bulk DOM parameters were correlated with DBP formation for different DBP classes to validate that we see the same trends that have been described previously in the literature. The bulk parameters assessed included DOC, as a measure of carbonaceous precursors, TDN, as a measure of nitrogenous precursors and a proxy for hydrophilic DOM fractions, SUVA-254 as a proxy for aromatic

and hydrophobic DOM fractions, and E2/E3 ratio as a proxy for DOM reactivity.[9,39,44] We considered the following four classes of DBPs: volatile C-DBPs (THMs and haloketones), HAAs, volatile N-DBPs (haloacetonitrile and chloropicrin), and nitrosamines. We investigated changes in the ratios of the individual DBPs formed but observed consistent relative formation of the individual DBPs and so we chose to cluster them by class. We used a stepwise linear regression to relate bulk DOM parameters and DBP formation for the entire set of samples generated (n = 24).

C-DBP formation was well-predicted using bulk parameters, including DOC, SUVA-254, E2/E3 ratio, and TDN (Table 1). The formation of volatile C-DBPs (haloketones and THMs) and HAAs were each positively correlated with an interaction term between DOC and SUVA-254. This interaction term arose because, in our dataset, lower DOC values often corresponded to lower SUVA-254 values. The formation of C-DBPs was negatively correlated with TDN. This trend implies that, consistent with previous observations, hydrophilic and nitrogen-rich DOM fractions that tend to dominate microbial DOM isolates (EfOM and AOM) are not responsible for C-DBP formation. The formation of C-DBPs was also negatively correlated with E2/E3 ratio. The E2/E3 ratio is negatively correlated with electron donating capacity, which suggests a positive correlation between C-DBP formation and electron donating capacity. That is, DOM with a higher electron donating capacity is more readily oxidized by chlorine. Therefore, the increase in E2/E3 ratio (reduction in electron donating capacity) is consistent with the removal of easily oxidized compounds, which leads to a reduction in C-DBP formation.[26] Overall, the bulk parameters could account for 94% of the observed variability in volatile C-DBP formation and 96% of the observed variability of HAA formation. These correlations are consistent with previous observations,[6,7] suggesting our dataset exhibits broadly observed DBP formation phenomena.

Volatile N-DBP formation (halonitriles and chloropicrin) was not as readily predicted by bulk parameters (Table 1). The stepwise linear regression revealed that volatile N-DBP formation was positively correlated with TDN and negatively correlated with E2/E3 ratio. The positive correlation with TDN is reasonable, given that the presence of more nitrogenous organic compounds could indicate that more N-DBP precursors could be present.[9,45] A negative correlation with E2/E3 ratio can be interpreted as a positive correlation with electron donating capacity. This again is a reasonable interpretation as a greater electron donating capacity implies greater reactivity with oxidants like chlorine.[26] No correlation was observed between SUVA-254 and DOC, suggesting aromatic carbonaceous moieties are not major precursors for N-DBP formation.[9] Overall, TDN and E2/E3 ratio could only account for 52% of the observed variability in halonitrile and chloropicrin formation.[11] These bulk parameters, therefore, are limited in how well they predict N-DBP formation but are consistent with previous work. Thus, either new bulk parameters need to be developed, or a molecular level investigation is needed to understand what drives N-DBP formation during chlorination of DOM.

Bulk parameters could only explain a small amount of variation in nitrosamine formation across the sample set (Table 1). Nitrosamine formation was negatively correlated with DOC, positively correlated with TDN, negatively correlated with an interaction term between E2/E3 ratio and TDN, and negatively correlated with SUVA-254. These results suggest first that nitrosamine DOM precursors are nitrogenous and not carbonaceous, as expected.[9,44] Second, the negative correlation with SUVA-254 is consistent with aromatic compounds not being precursors for nitrosamines. Indeed, aromatic compounds could even suppress the formation of nitrosamines by competing for oxidants. Overall, these bulk DOM properties could account for only 39% of nitrosamine formation. However, it should be noted that nitrosamine formation was only observed in half of the samples tested (n = 12) and thus, the dataset is more limited for nitrosamines, compared to the other DBP classes. These results are generally consistent with known nitrosamine formation trends and establish that our dataset is broadly comparable with the known literature.

We next examined how the sequence of water treatment steps impacted the formation of classes of DBPs for each of the DOM isolates. The formation of C-DBPs generally responded to treatment as expected for SRFA. SRFA had the highest formation of THMs and HAAs, followed by EfOM and AOM (Fig. 2A–C, leftmost bars). Permanganate pre-oxidation alone did not impact the formation of total THMs or HAAs for SRFA, but permanganate pre-oxidation did lead to a greater decrease in THM and HAA formation from SFRA in the subsequent alum coagulation step, compared to alum

Table 1 Summary of stepwise linear regression analysis

	C-DBPs				N-DBPs			
	Volatiles		Haloacetic acids		HANs & CP		Nitrosamines	
	B	*p*	*B*	*p*	*B*	*p*	*B*	*p*
DOC	—	—	—	—	—	—	−21	0.0001
TDN	−495.9	0.0001	−567.7	0.0002	20.6	0.0004	—	—
SUVA-254	—	—	—	—	—	—	−69	0.005
E2/E3 ratio	−13.1	0.001	−22.2	0.00002	−0.4	0.028	—	—
DOC × SUVA-254	7.7	0.036	19.0	0.0002	—	—	—	—
TDN × E2/E3 ratio	—	—	—	—	—	—	−30.0	0.012
Adjusted R^2	**0.94**		**0.96**		**0.52**		**0.39**	

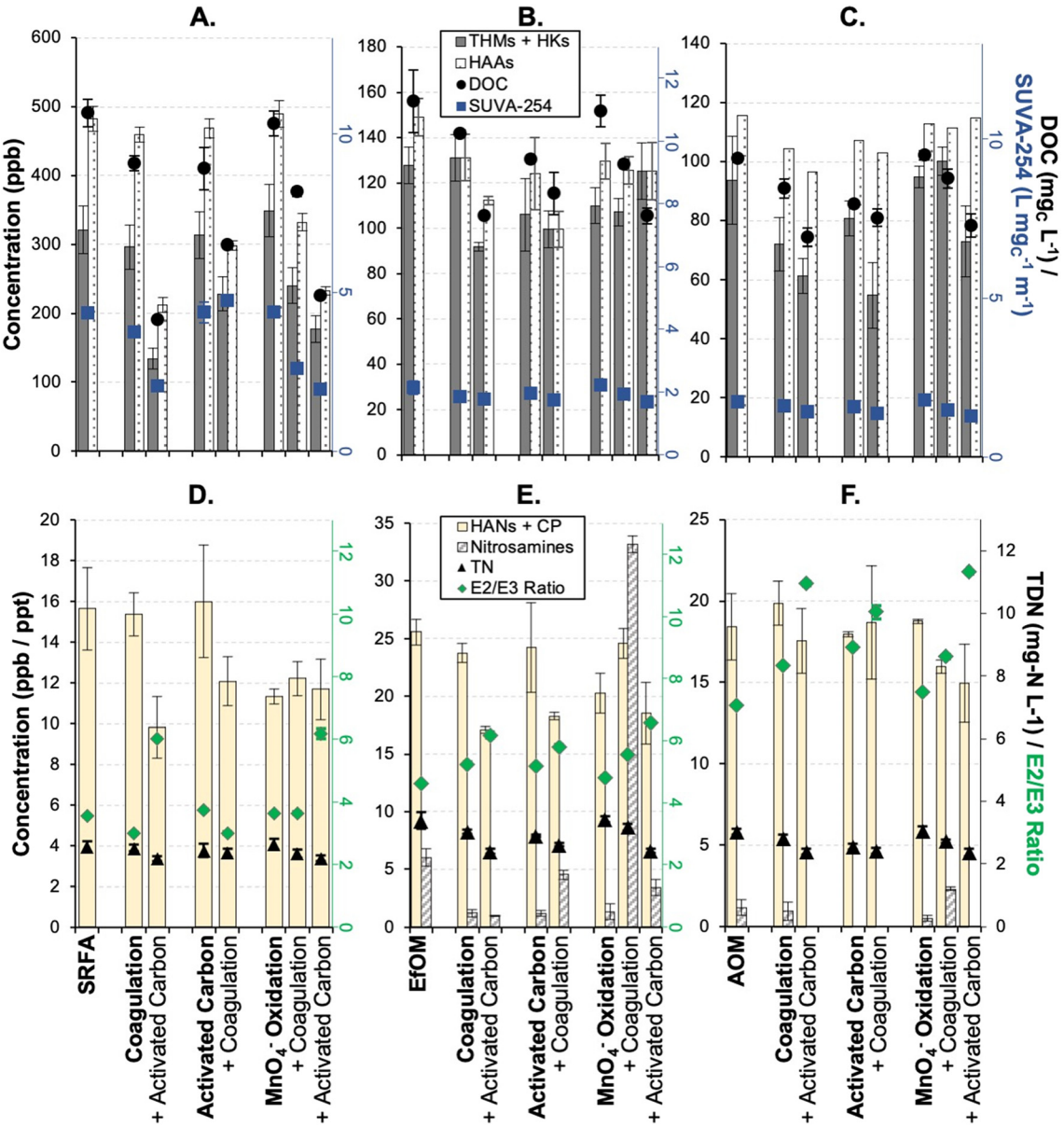

Fig. 2 Impact of treatment on the formation of C-DBPs (grey bars for THMs and HKs, white bars with dots for HAAs, A–C), N-DBPs (yellow bars for HANs and CP, grey and white striped bars for nitrosamines, D–F), alongside bulk properties (A–C: DOC (black circles) and SUVA-254 (blue squares); D–F: TDN (black triangles)) and E2/E3 ratio (green diamonds) for each isolate: SRFA (A & D), EfOM (B & E), AOM (C & F). Note the change in scale across *y*-axes in each subfigure.

coagulation applied alone (Fig. 2A). A second subsequent treatment of activated carbon further decreased total C-DBPs for SRFA to levels similar to coagulation-plus-activated carbon treatment, whether or not permanganate pre-oxidation was applied, and lower than activated carbon as the sole treatment step. In contrast, C-DBP formation trends for microbial isolates differed from SRFA and also between the two sources and between THM and HAA classes.

Overall, treatment steps for EfOM and AOM showed little change in HAA formation and only a few instances of decreases in THM formation, compared to the original DOM. Permanganate oxidation showed a slight decrease in C-DBP formation for EfOM and no change for AOM (Fig. 2B and C). Coagulation treatment only showed a change in C-DBP formation when applied as the first treatment and only for AOM (Fig. 2B and C). Activated carbon treatment did reduce THMs only after the treatment sequence with permanganate oxidation and only for AOM. Although each DOM type showed similar patterns of changes in DOC levels (Fig. 2, black circles) for the various treatment steps within a sequence, the trends in SUVA-254 (Fig. 2, blue squares) were better correlated with total C-DBP formation, as established in the preceding regression analysis. Overall, the greatest reduction in THM formation from SRFA and EfOM was achieved by the sequence of alum coagulation followed by activated carbon sorption (Fig. 2A and B). For AOM, the most

effective sequence was activated carbon followed by alum coagulation (Fig. 2C). The most effective treatments for removing HAA precursors differed slightly. For SRFA and AOM, the greatest reduction in HAA formation was observed in the sequence where alum coagulation was followed by activated carbon sorption. For EfOM, the permanganate pre-oxidation sequence was the most effective in reducing HAA formation.

Treatment steps had different impacts on N-DBP formation than for C-DBP formation and these trends varied by DOM source type (Fig. 2D–F). The formation of volatile N-DBPs (HANs-plus-chloropicrin) was the greatest for EfOM samples, with lower, and comparable, formation for the SRFA and AOM samples. Permanganate pre-oxidation decreased N-DBP formation from SRFA and EfOM but did not alter the volatile N-DBP formation from AOM (Fig. 2D–F). Permanganate pre-oxidation resulted in no change in volatile N-DBP formation after coagulation for SRFA, an increase in N-DBP formation for EfOM, and a decrease for AOM; whereas coagulation applied as the first treatment step did not cause a change in formation of volatile N-DBPs for any DOM sources (Fig. 2D–F). Activated carbon treatment reduced volatile N-DBP formation following a previous treatment, but not as the first treatment step. Overall, the reduction in N-DBP formation from SRFA and EfOM was comparable for all treatment sequences, but only permanganate pre-oxidation followed by alum coagulation resulted in a reduction in N-DBP formation for AOM. Additionally, resulting decreases in TDN and increases in E2/E3 ratio generally correlated with the formation of N-DBPs, consistent with our prior regression analysis. Like C-DBPs, the impact of treatment on volatile N-DBP formation varied with DOM source type.

Nitrosamine formation showed similar trends as volatile N-DBPs across treatment steps, with activated carbon sorption being the most effective treatment strategy (Fig. 2D–F). The highest formation of nitrosamines was from the EfOM isolate, followed by the AOM isolate. No nitrosamine formation was observed from the chlorination of SRFA, likely due to its lower dissolved nitrogen content. The formation of nitrosamine in our experimental samples likely is not environmentally relevant, as the chlorine addition aimed to maximize the formation of these DBPs so we could evaluate precursor removal, rather than to simulate chlorination in distribution systems. Permanganate oxidation decreased the formation of nitrosamines for both microbial isolates. Subsequent coagulation increased nitrosamine formation for both EfOM and AOM, which may be due to greater total carbon removal compared to total nitrogen removal. Removal of carbonaceous DOM may have led to a shift in the moieties available for reaction towards those that are nitrogenous, a phenomenon that has been observed previously for other DOC removal processes.[19–22] Nitrosamine formation decreased when activated carbon sorption followed permanganate pre-oxidation and alum coagulation. For both microbial isolates, activated carbon sorption always reduced nitrosamine formation while alum coagulation sometimes increased nitrosamine formation. Although the dataset for nitrosamines is smaller, there are consistent trends in how nitrosamine precursors are altered by treatments, regardless of DOM isolate source type.

Ion type provides greater insight in DOM molecular level characterization

The formation of DBPs from the different DOM isolates responded very differently to the same applied treatments. The application of molecular level tools, as opposed to bulk properties, can provide insights to understand why the responses were different. We chose to use FT-ICR-MS to identify the components in the initial sample that reacted fully with chlorine, meaning the chemical formula was present in the mass spectrum of the initial isolate but it was absent in the mass spectrum of the isolate obtained after chlorination (signal intensity was reduced by 100%). We then compared these components with those removed by each treatment step, meaning the chemical formula was present in the mass spectrum of the DOM sample before treatment but not in the mass spectrum of the DOM after treatment (signal intensity was reduced by 100%). We believe this is a conservative approach to identify components removed by treatment and suspect DBP precursors and to minimize false DBP precursor identification caused by ion suppression. In this way, we identified components removed by treatment that react fully with chlorine, and we call them suspect DBP precursors.

We enhanced our characterization of DOM by using multiple ionization techniques and by identifying the types of ions formed, to gain insight into possible chemical structures of the suspect DBP precursors.[29,46] In negative ion mode, we observed pseudo-molecular ions ($[M - H]^-$) formed by the loss of a proton and molecular ions ($[M\cdot]^-$) formed by reduction. Pseudo-molecular ions must contain an acidic functional group that deprotonates readily, such as a phenol or alcohol moiety.[47] Molecular ions, in contrast, must be stable as a radical anion, such as quinone structures.[48,49] In positive ion mode, we considered the formation of pseudo-molecular ions ($[M + H]^+$) formed by the gain of a proton, molecular ions ($[M\cdot]^+$) formed by oxidation, and sodium adducts ($[M + Na]^+$) formed by coordination with sodium. In positive ion modes, pseudo-molecular ions are formed by basic functional groups that can readily accept a proton to become positively charged and can include benzoic acids and amines. Molecular ions can arise from quinones or iminoquinones in positive ion modes.[47,50,51] Sodium adducts require a site where the positively charged sodium ion can coordinate, and thus these components may contain diether or dicarbonyl structures.[52,53] ESI was used to ionize soluble, non-aromatic components while LDI was used to target aromatic compounds.[47] The data is presented in van Krevelen diagrams, with chemical formulae distinguished by the ion type by which they were observed (Fig. S1). We present an

overview of the van Krevelen diagrams for the initial DOM samples and subsequent treatments in Fig. S2–S4 and van Krevelen diagrams of the suspect DBP precursors for every sample in Fig. S5–S7. We focus on understanding how permanganate oxidation impacts DBP formation in the drinking water treatment sequence and then identify which DBP precursors were impacted by the most effective treatments. By considering how the ions were observed, we

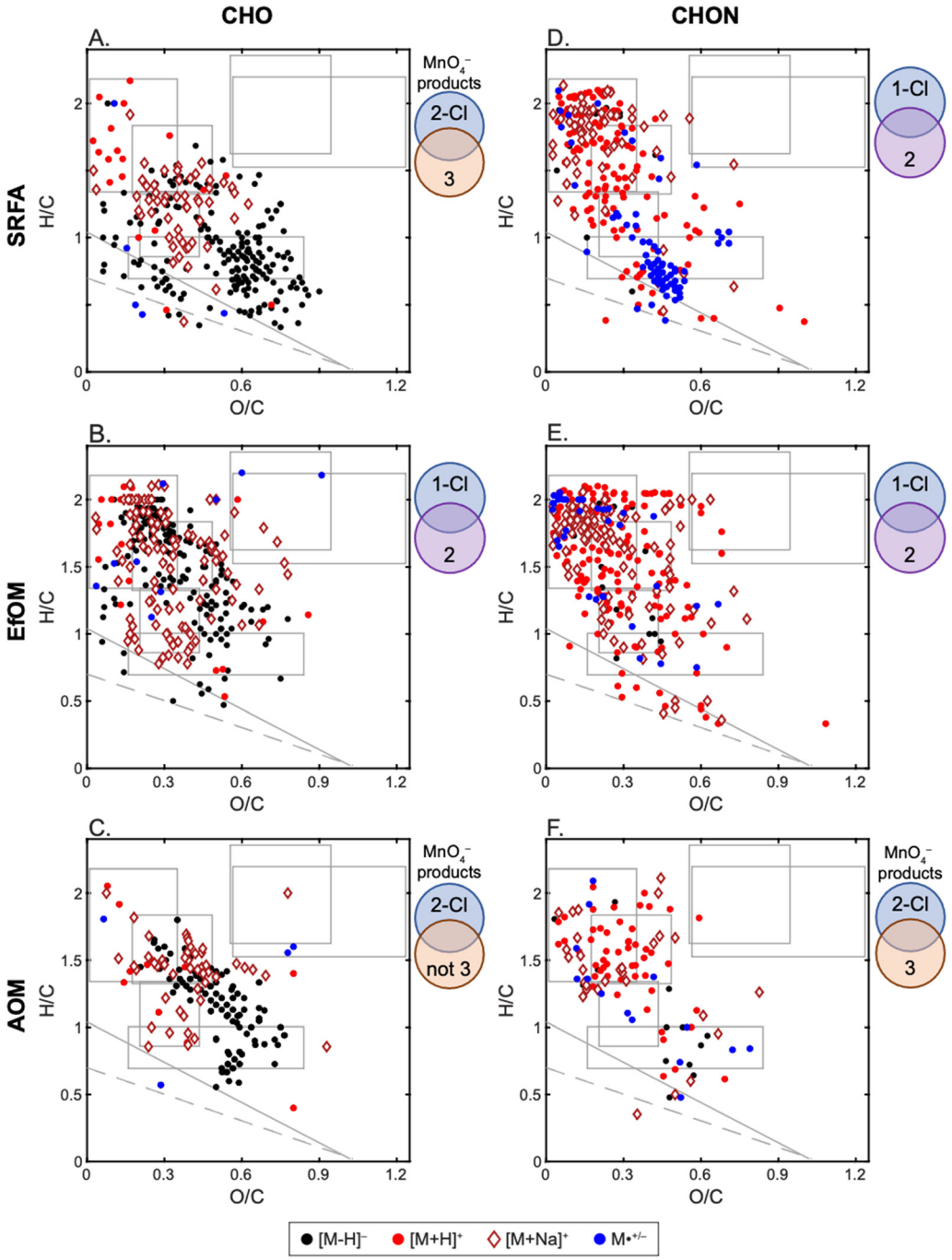

Fig. 3 Molecular level insights into the impact of permanganate pre-oxidation on DBP precursors. DOM components are separated by ion type: $[M - H]^-$ as black circles, $[M + H]^+$ as red circles, $[M + Na]^+$ as dark red diamonds, and $M^{\cdot +/-}$ as blue circles. Venn diagrams using the treatment numbering scheme presented in Fig. 1 are provided to the right of each diagram to describe the comparison being made. A. CHO permanganate oxidation products from SRFA that both react fully with chlorine (are DBP precursors) and were removed by subsequent coagulation. B. CHO components in the initial EfOM sample that reacted fully with both chlorine and permanganate. C. CHO permanganate oxidation products from AOM that reacted fully with chlorine and were not removed by subsequent coagulation treatment. D. CHON components in the initial SRFA sample that reacted fully with both chlorine and permanganate. E. CHON components in the initial EfOM sample that reacted fully with both chlorine and permanganate. F. CHON permanganate oxidation products from AOM that reacted fully with chlorine and were removed by subsequent coagulation treatment.

obtained deeper insight into how DOM isolates changed during treatment and how these changes impacted DBP formation.

Permanganate pre-oxidation impacts removal of C-DBP precursors by coagulation

Permanganate pre-oxidation of SRFA resulted in lower C-DBP formation following alum coagulation because it improved the removal of C-DBP precursors from SRFA by subsequent alum coagulation (Fig. 2A & 3A). We examined the CHO formulae that were formed by permanganate oxidation (MnO_4^- products) and also reacted fully with chlorine. Previously, it was observed that permanganate oxidation improved the removal of aromatic components in SRFA through the addition of oxygen-containing functional groups.[29] These components were observed as tannin-like pseudo-molecular anions with high oxygen-to-carbon ratios and as lignin-like sodium adducts, which are likely oxidized ring-opening products.[29] Herein, we found that the permanganate oxidation products that also fully reacted with chlorine showed the same ion characteristics (Fig. 3A), which supports the role of these DOM components as DBP precursors. These findings also suggest that permanganate oxidation of DOM components does not fully remove potential for their reaction with chlorine and thus, the reactive site for chlorine on these components differs from the reactive site with permanganate. Overall, the impact of permanganate "pre-oxidation" on terrestrial SRFA was to alter aromatic DOM precursors so they are more effectively removed in subsequent treatment, rather than to preferentially oxidize components in advance of chlorination as a disinfection step.

Permanganate oxidation of EfOM reduced the formation of C-DBPs through oxidation of the precursor DOM components by permanganate (Fig. 2B & 3A). Previously, we observed that permanganate preferentially oxidized lipid-, peptide-, and lignin-like components to form oxidized products that included quinones.[29] We compared the CHO components from EfOM that were oxidized by permanganate with those EfOM components that reacted fully with chlorine (Fig. 3B). Chlorine reacted with similar components as permanganate, components that are lipid- and peptide-like and, to a lesser extent (based on the relative abundances in each region), lignin-like. These observations suggest that both oxidants react with the same EfOM moieties, which include peptides and to a lesser extent phenols. EfOM contains fewer aromatic components and therefore precursors than SRFA and thus, the impact of subsequent coagulation was not as important to C-DBP precursor removal as it was for SRFA. Overall, in the case of EfOM, permanganate did behave as a pre-oxidant whereby it reacted with moieties susceptible to chlorination, which resulted in a reduction of C-DBP formation.

In contrast to SRFA and EfOM, permanganate oxidation neither oxidized C-DBP precursors in AOM nor improved their removal from AOM by subsequent alum coagulation (Fig. 2C & 3C). Previously, we observed that permanganate oxidation improved the removal of DOC, especially aromatic DOC, from AOM.[29] Thus, we expected to observe a greater decrease in C-DBP formation compared to alum coagulation applied alone. Our observation of no change in C-DBP formation between permanganate-treated and permanganate-plus-coagulation treatment suggests that the components removed by alum coagulation following permanganate oxidation are not C-DBP precursors. We identified permanganate oxidation products that are not removed by alum coagulation and that also react fully with chlorine (Fig. 3C). These components tended to be less aromatic in character but may still contain phenolic moieties observed as $[M - H]^-$ tannin-like components. Many of the components were peptide-like dicarbonyls observed as $[M + Na]^+$ adducts. Taken together, these observations suggest that permanganate reacts with different AOM moieties than chlorine and the components with chlorine reaction sites are less susceptible to alum coagulation compared to other products of AOM permanganate oxidation. Overall, the impact of permanganate pre-oxidation on C-DBP formation was different for each isolate tested and reflected differences in their initial DOM molecular composition.

Permanganate pre-oxidation generally reduces N-DBP formation potential

Permanganate oxidation of SRFA decreased N-DBP formation potential by oxidizing N-DBP precursors (Fig. 2D & 3D). Permanganate pre-oxidation reduced N-DBP formation without decreasing TDN, suggesting that permanganate oxidation reduces the overall reactivity of chlorine with nitrogenous organic compounds. Previously, it was found that permanganate preferentially oxidizes nitrogenous components including those that are lipid-like, peptide-like and tannin-like aromatic components.[29] This trend is consistent with amine functional groups acting as an activating group by increasing electron density at aromatic rings or double bonds.[28] We identified the CHON components that reacted fully with both permanganate and chlorine (Fig. 3D) and found that these same SRFA components that were known to react with permanganate are also likely N-DBP precursors. Overall, these trends support the use of permanganate as a DBP control strategy by lessening the reactivity of nitrogenous organic components.

Permanganate treatment of EfOM also reduced the formation of N-DBPs by oxidation of precursor components, although the component characteristics showed some differences from SRFA (Fig. 2E & 3E). It was previously observed that permanganate reacted with nitrogenous lignin-like, as well as lipid and peptide-like components in EfOM. Again, this preferential reaction with nitrogen-containing compounds is consistent with permanganate reactivity trends. When the components that reacted fully with permanganate and chlorine are compared, it is revealed the

two oxidants target similar components, particularly those that are peptide- and lignin-like (Fig. 3E). Interestingly, subsequent alum coagulation resulted in an increase in N-DBP formation. Taken together, this suggests that the components that were oxidized by permanganate can still react with chlorine, but with lower reactivity. These

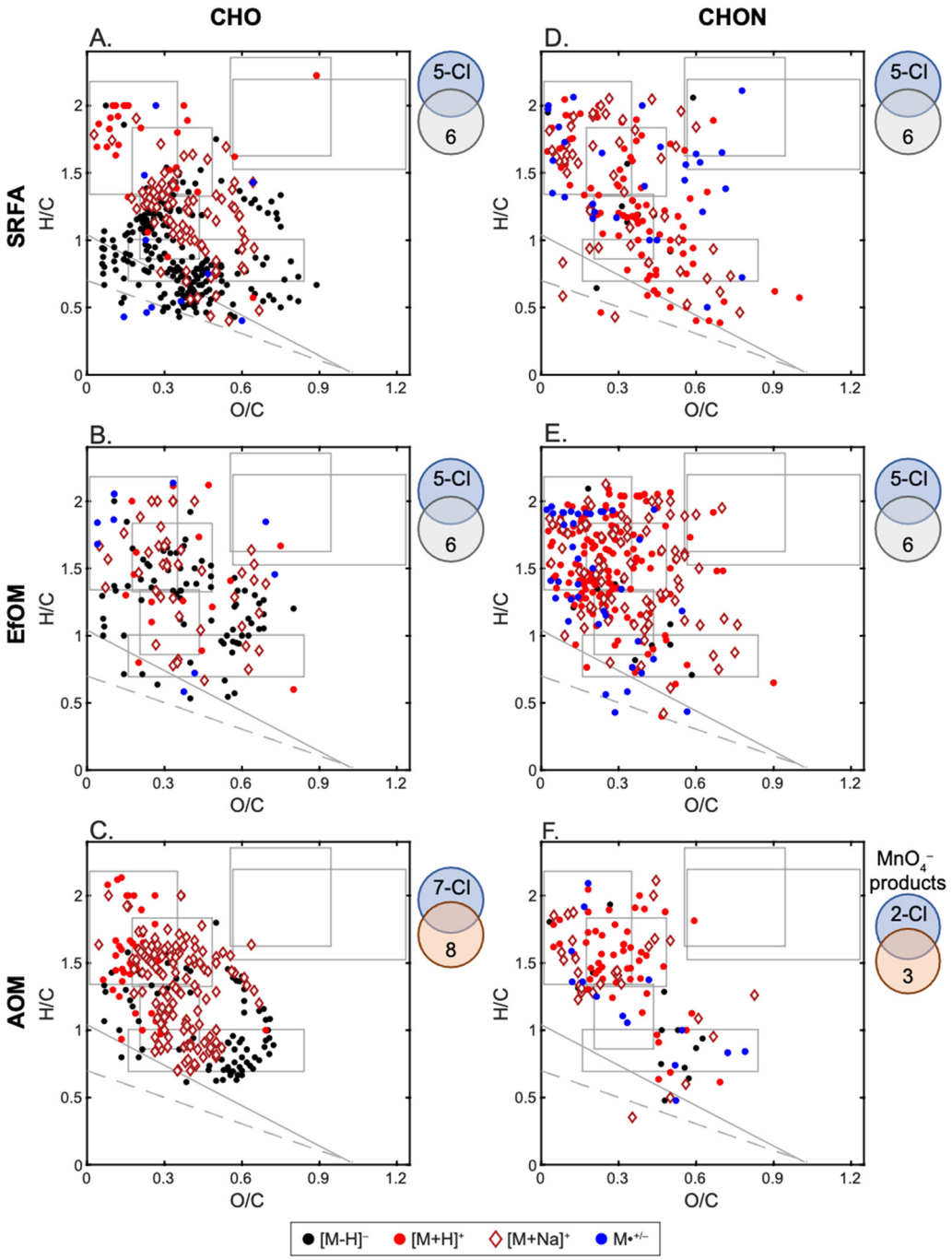

Fig. 4 DBP precursors (formula that are absent after chlorination) that are removed by the most effective treatment for each isolate. Data is presented for the most effective treatment step for each isolate. DOM components are separated by ion type: $[M - H]^-$ as black circles, $[M + H]^+$ as red circles, $[M + Na]^+$ as dark red diamonds, and $M^{\cdot+/-}$ as blue circles. Venn diagrams using the treatment numbering scheme presented in Fig. 1 are provided to the right of each diagram to describe the comparison being made. A. CHO precursors in SRFA that are present after coagulation and removed by activated carbon sorption following coagulation. B. CHO precursors in EfOM that are present after coagulation and removed by activated carbon sorption following coagulation. C. CHO precursors in AOM that are present after activated carbon sorption and removed by coagulation following activated carbon sorption. D. CHON precursors in SRFA that are present after coagulation and removed by activated carbon sorption after coagulation. E. CHON precursors in EfOM that are present after coagulation and removed by activated carbon sorption following coagulation. F. CHON permanganate oxidation products in AOM that are also N-DBP precursors and removed by alum coagulation following permanganate pre-oxidation.

nitrogenous components may have become more important for reaction with chlorine after coagulation treatment removed more DOC than TDN and hence lowered the availability of chlorine-reactive carbonaceous compounds.

Permanganate oxidation alone did not reduce the formation of N-DBPs from AOM, but permanganate oxidation did improve the removal of N-DBP precursors in subsequent alum coagulation (Fig. 2F & 3F). Previously, we observed that permanganate preferentially reacted with nitrogenous components in AOM, including peptide- and lipid-like components and lignin-like components, consistent with permanganate reactivity trends.[29] The oxidation of these components may have improved their removal by alum coagulation and this may have occurred through preferential interactions with coagulation flocs compared to C-DBP precursors because permanganate oxidation was associated with little change in C-DBP formation after subsequent coagulation.[29] We compared CHON permanganate oxidation products removed by alum coagulation with permanganate oxidation products that reacted fully with chlorine to identify AOM suspect N-DBP precursors removed by alum coagulation (Fig. 3F). We observed that the suspect N-DBP precursors were mainly lipid- and peptide-like, with a few highly oxidized tannin-like components. Although the underlying reasons for the reduction of N-DBP formation differs between the isolates, these trends support using permanganate pre-oxidation as a strategy to control N-DBP formation.

Combined activated carbon and coagulation are most effective in reducing C-DBP formation potential

We examined the treatment sequences that showed the most promise in reducing the total DBP formation potential for a given DOM source type. In each case, the reduction in DBP formation potential, compared to the source organic matter, could be attributed to a single step in the treatment sequence. For SRFA, activated carbon sorption applied after alum coagulation was the most effective treatment step for removing C-DBP precursors (Fig. 2A) because of improved removal of aromatic DOM components. We compared the CHO components in SRFA that were suspect C-DBP precursors remaining after alum coagulation with the components removed by activated carbon sorption when the step followed alum coagulation (Fig. 4A). Previously, it was observed that lipid-like components are preferentially removed in the first, alum coagulation, treatment step.[29] Removal of these lipid-like components, may have improved access to activated carbon sorption sites for C-DBP precursors. We note that activated carbon applied as a first treatment had no net effect on the formation of C-DBPs from SRFA (Fig. 2A). In general, SRFA components with lower O/C and H/C ratio were removed by activated carbon sorption following coagulation and these components reacted fully with chlorine indicating their importance as DBP precursors. This trend suggests that hydrophobic interactions drove the removal of C-DBP precursors in the activated carbon treatment step. Additionally, these components were observed as $[M - H]^-$, further supporting the role of phenols as C-DBP precursors and consistent with the broader literature.[8]

The most effective treatment step to remove C-DBP precursors from EfOM was also activated carbon sorption following alum coagulation. We again identified the suspect C-DBP precursors remaining after alum coagulation and that were removed by activated carbon sorption following alum coagulation (Fig. 4B). Similar components, including $[M - H]^-$, likely phenolic components, were removed by this treatment step. However, this treatment strategy was less effective for C-DBP precursors in EfOM than for C-DBP precursors in SRFA. Instead, more aliphatic and oxidized EfOM components, that appeared as $[M + Na]^+$ adducts, were removed by activated carbon sorption after alum coagulation. This trend suggests there may be a different adsorption mechanism for EfOM components. Overall, these observations support that the C-DBP precursors differ between SRFA and EfOM and underscores why the two different DOM isolates responded differently to treatment.

In contrast, the most effective treatment step to remove C-DBP precursors from AOM was alum coagulation following activated carbon sorption. Coagulation improved removal of aromatic tannin-like components and oxidized lignin- and peptide-like components. Analogously, we compared the AOM components that remained as C-DBP precursors after activated carbon sorption with components that were fully removed by alum coagulation when it followed activated carbon sorption (Fig. 4C). This analysis revealed that coagulation preferentially removed aromatic tannin-like components, ions that were observed as $[M - H]^-$ suggesting they may be phenolic. Further, dicarbonyl peptide- and lignin-like components that were observed as $[M + Na]^+$ ions were also removed by alum coagulation. These dicarbonyl species may have improved polar and electrostatic interactions with the alum flocs. This improved removal compared to coagulation applied alone may have been due to the initial removal of abundant lipid- and peptide-like components by the activated carbon treatment step. Overall, the C-DBP precursors in AOM appear to be more similar to SRFA than EfOM and implicates terrestrial materials, like lignin and tannin molecules, as being responsible for C-DBP formation in this environmental isolate. Collectively, these observations highlight that different effects of common water treatment steps to reduce DBP formation resulted from differences in the characteristics of the C-DBP precursors across DOM types.

Combined activated carbon and coagulation are most effective in reducing N-DBP formation potential

Activated carbon sorption following alum coagulation was the most effective treatment step to remove N-DBP precursors from SRFA, as was also the case for removal of C-DBP precursors from SRFA. We identified CHON N-DBP

precursors that remained after alum coagulation and were removed by activated carbon sorption following coagulation (Fig. 4D). These suspect N-DBP precursors included aromatic amines that were observed as $[M + H]^+$ ions with low H/C ratios. There were also lipid-like components that appeared as $[M + Na]^+$ adducts, suggesting compounds containing dicarbonyl moieties may also be responsible for N-DBP formation. The effectiveness of alum coagulation-plus-activated carbon for reducing N-DBP formation was comparable to permanganate oxidation as a sole treatment step (Fig. 2D). These observations highlight that both sorptive removal and oxidative strategies can be equally effective treatments to reduce N-DBP formation potential from terrestrial-derived DOM.

The most effective treatment step to remove N-DBP precursors from EfOM was activated carbon sorption following alum coagulation, as was also the trend for C-DBP removal from EfOM. Analogously, we compared CHON N-DBP precursors that were present after coagulation with those removed by activated carbon sorption after alum coagulation (Fig. 4E). This analysis revealed that basic moieties, that were ionized using positive ion modes, were likely responsible for N-DBP formation. A mixture of aromatic and lipid-/peptide-like components were identified. Some of these components likely contained dicarbonyl or diester moieties due to their appearance as $[M + Na]^+$ ions. These functional groups may be involved in polar interactions with activated carbon sorption sites. The N-DBP precursors abundant in EfOM differed from those for SRFA, although the same treatment sequence was effective to achieve the greatest reduction in N-DBP formation. EfOM N-DBP precursors were more aliphatic (higher H/C ratios) in character compared to SRFA, which is consistent with SUVA-254 not being predictive of N-DBP formation.

In contrast, the most effective treatment step to remove N-DBP precursors from AOM was alum coagulation following permanganate oxidation which led to the greatest decrease in N-DBP formation for AOM (Fig. 2F). We identified CHON N-DBP precursors that were formed during permanganate oxidation of AOM and were also removed by alum coagulation following permanganate pre-oxidation (Fig. 4F). Most of the components susceptible to both oxidative strategies were lipid- and peptide-like components that appeared as sodium adducts. This is again consistent with SUVA-254 being a poor predictor of N-DBP formations. There were fewer aromatic components identified as suspect N-DBP precursors in AOM compared to SRFA and EfOM. These components were also distinct from those in SRFA and EfOM because they appeared as deprotonated ions, indicating the presence of an acidic functional group in these compounds. Overall, these differences in response to treatment suggest the N-DBP precursors present in each of the DOM isolates are unique and that sorptive processes are effective removal strategies.

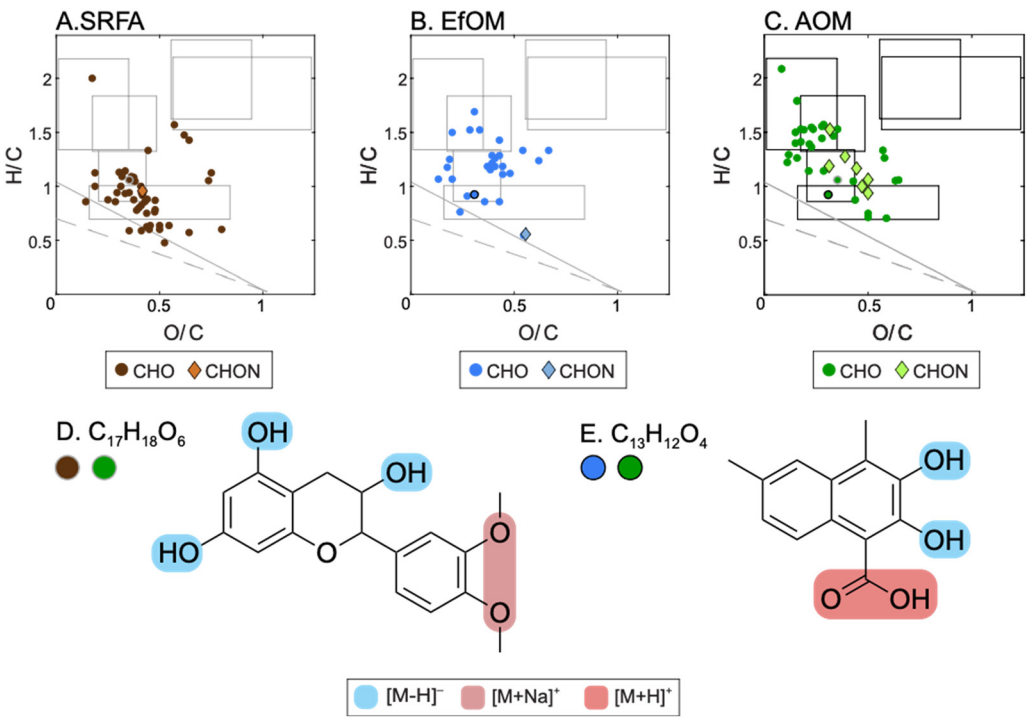

Fig. 5 DOM components that were not removed by any applied treatments, but always reacted fully with chlorine for A. SRFA, B. EfOM, and C. AOM. Components are separated into CHO formulae (dark circles) and CHON formulae (lighter diamonds). The common formula are circled in grey (D) and black (E), in their respective van Krevelen diagrams. Proposed structures for two common DBP precursor formulae that are not removed by any treatments studied here. The ionization sites are highlighted on each molecule. D. Epicatechin 3′,4′-dimethyl ether for $C_{17}H_{18}O_6$ E. 2,3-dihydroxy-4,6-dimethylnaphthalene-1-carboxylic acid for $C_{13}H_{12}O_4$.

Persistent DBP precursors exhibit similar characteristics across DOM from different sources

Persistent suspect DBP precursors that were not removed by treatment were identified for each of the DOM isolates (Fig. 5A–C). Overall, there were 2035 formulae identified as DBP precursors that reacted fully with chlorine in the initial SRFA sample, 1576 formulae in the initial EfOM sample, and 1584 formulae in the initial AOM sample. We narrowed these formulae to those that were found in every sample following treatment. Thus, it is unlikely that these components disappeared by chance, and it is likely that these components would persist through treatment. All DOM isolates contained CHO DBP precursors that were lignin-like. SRFA and AOM both contained persistent CHO DBP precursor tannin-like components, likely from terrestrial origins. EfOM and AOM both contained peptide-like precursors and precursors that were more oxidized than lignin and peptides, suggesting these arise from microbial origins. We considered two chemical formulae that were each common between two isolates in greater detail: $C_{17}H_{18}O_6$ and $C_{13}H_{12}O_4$.

Using the observed ion types for the formula, we propose epicatechin 3′,4′-dimethyl ether as a plausible chemical structure for $C_{17}H_{18}O_6$ (Fig. 5D). This chemical formula was present in both SRFA and AOM, suggesting it arises from terrestrial origins, as our AOM sample was from a lake that presumably had some terrestrial inputs from the surrounding land. It was ionized by negative mode ESI as a $[M - H]^-$ ion, meaning it must contain an acidic proton that yields a stable anion. The proposed epicatechin structure contains two phenolic hydrogens as well as a benzyl alcohol, all of which have high gas-phase acidity.[54] The compound was also observed by positive mode ESI as a sodium adduct, meaning the structure must contain a site where the positively charged sodium ion can be stabilized. In the proposed structure, there is a diether, which could stabilize a positive charge. While this structure is not the only possibility (1400 possibilities on Pubchem), it highlights which substructures we expect. Interestingly, the chemical formula, $C_{17}H_{18}O_6$, was also present in EfOM, but it did not react with chlorine. This highlights that even though the chemical formula is the same, it likely has a different structure and further supports the assignment of a plant metabolite in SRFA and AOM.

We propose 2,3-dihydroxy-4,6-dimethylnapthalene-1-carboxylic acid as a structure for $C_{13}H_{12}O_4$, based on the observed ion types (Fig. 5E). This chemical formula was present in both EfOM and AOM. It was ionized by negative mode ESI as $[M - H]^-$, suggesting it has an acidic proton. It was also ionized in AOM by positive mode ESI as $[M + H]^+$, suggesting the presence of a basic functional group. However, because it is not universally observed by positive mode ESI, it suggests the functional group has a lower proton affinity and is subject to ion suppression. The proposed structure contains two phenolic hydroxyl groups that could form a pseudo-molecular anion ($[M - H]^-$). It also contains a carboxyl moiety that would have a lower proton affinity due to the presence of the hydroxyl groups. The methyl and aromatic groups both increase gas phase acidity to support deprotonation of the hydroxyl groups. Again, this structure is not the only possibility (2600 possibilities on Pubchem), but many other structures lack a basic functional group, and many have quinone moieties, which would be expected to appear as radical anions. The proposed structure highlights the expected substructures, and that ion types can be used to eliminate some possible structures.

Conclusions

Managing DBP formation remains an ongoing challenge for drinking water utilities to provide high quality drinking water. Here, we attempted to provide insight into the different DBP precursors contained within different types of DOM, why different DOM isolates respond differently to typical drinking water treatments, and which DBP precursors persist through treatment. For C-DBPs, we observed correlations with organic carbon content and SUVA-254 (a proxy for aromaticity) and C-DBP formation, consistent with previous literature observations. However, we observed differences in the chemical signature of the DBP precursors identified by ultrahigh resolution-mass spectrometry for the different isolates. In SRFA, we observed C-DBP precursors that were dominated by aromatics, tannin-like, and lignin-like formula. The C-DBP precursors in EfOM were more aliphatic in character (higher H/C ratios) represented by lipid- and peptide-like formula, presumably due to the lower abundance of aromatics in EfOM. AOM, which contains both terrestrial and microbial inputs, had signatures of both C-DBP precursor types.

Analogously, N-DBP precursors differed for the different DOM isolates. We observed correlations between TDN and DOM reactivity (as approximated by E2/E3 ratios) consistent with prior literature. Our methods were especially suited to detect nitrogenous components because we employed positive ionization modes, which readily ionize amines. We observed for SRFA that N-DBP precursors were distributed among many chemical classes, including aromatic, tannin-, lignin-, peptide, and lipid-like components. EfOM contained N-DBP precursors that were more densely clustered in the lipid- and peptide-like chemical classes. AOM, again, contained a mixture of both N-DBP precursors with lipid and peptide-like N-DBP precursors being among the most dominant. The different abundances of DBP precursors led to differences in how the isolates responded to treatment.

In general, a combination of activated carbon and alum coagulation was the most effective in reducing DBP formation, but in some cases comparable reductions were observed for permanganate oxidation. The underlying molecular level reasons for why these treatments were effective differed with DOM isolate. For example, SRFA and EfOM had the greatest reduction in C-DBP and N-DBP formation when activated carbon followed alum coagulation,

but the reduction in SRFA was driven by improved removal of aromatic, tannin-like, and lignin-like DBP precursors while the reduction in EfOM was driven by improved removal of highly oxidized species and lignin- or peptide-like components. In the case of permanganate oxidation, permanganate sometimes directly oxidized DBP precursors (as was the case C-DBP precursors in EfOM and N-DBP precursors in SRFA and EfOM) and other times improved the removal of DBP precursors by subsequent sorption processes (for example, C-DBP precursors in SRFA and N-DBP precursors in AOM). Overall, the results highlight the complexity in the molecular changes induced by treatment but support the use of combined activated carbon and coagulation strategies to reduce DBP formation and the use of permanganate oxidation to reduce DBPs, especially N-DBPs.

Finally, we demonstrated how ultrahigh resolution-mass spectrometry (*i.e.*, FT-ICR-MS) can be used as a screening tool to identify important DOM components. Ultrahigh resolution-mass spectrometry can be used in a more comprehensive way to identify chemical formulae of interest through absence/presence analyses and by using multiple ionization techniques. How the chemical formulae appear in the mass spectra, namely, their ion type provides hints about their underlying chemical structure. We have demonstrated how this information can be used not only to understand transformation and removal processes but also to propose chemical structures for persistent DBP precursors. Future work should focus on conclusively identifying these DOM components that are susceptible to chlorination but are not removed by treatment using liquid chromatography with tandem mass spectrometry. Similar approaches can be used to understand DOM oxidation or sorption processes in both natural and engineered systems.

Author contributions

JRL was responsible for conceptualization, method development, data acquisition, data analysis and interpretation, writing the first draft, and revising subsequent drafts. AAK contributed to conceptualization, supervision, data interpretation, and manuscript revision.

Conflicts of interest

There are no conflicts to declare.

List of abbreviations

ACS	American Chemical Society
AOM	Algal-derived organic matter
C-DBPs	Carbonaceous disinfection byproducts
DBPs	Disinfection byproducts
DOC	Dissolved organic carbon
DOM	Dissolved organic matter
EfOM	Wastewater effluent-derived organic matter
EPA	Environmental Protection Agency
ESI	Electrospray ionization
FT-ICR-MS	Fourier transform-ion cyclotron resonance-mass spectrometry
GC-MS	Gas chromatograph-mass spectrometer
HAAs	Haloacetic acids
$KMnO_4$	Potassium permanganate
LC-MS	Liquid chromatography-mass spectrometry
LDI	Laser desorption/ionization
MTBE	Methyl *tert*-butyl ether
N-DBPs	Nitrogenous disinfection byproducts
PAC	Powdered activated carbon
PPL	Agilent Bond Elut Priority Pollutant
PVDF	Polyvinylidene fluoride
SRFA	Suwannee river fulvic acid
SUVA-254	Specific ultraviolet absorbance at 254 nm
THMs	Trihalomethanes
TDN	Total dissolved nitrogen
UV-vis	Ultraviolet-visible

Data availability

The data supporting this article have been included as part of the supplementary information (SI). Raw data files and formula assignments are available upon request from JRL.

Supplementary information: including DOM characterization, FT-ICR-MS methodology, DBP quantification, additional overview van Krevelen diagrams, and solution parameters. See DOI: https://doi.org/10.1039/d5ew01131k.

Acknowledgements

We thank the late Prof. Dion Dionysiou for granting us access to his GC-MS. The analysis of volatile C-DBPs would not have been possible without his willingness to open his lab to us. We thank his student, Minghao Kong, for queuing samples and sending data to us. We thank our anonymous reviewers for improving the clarity of this work. We acknowledge financial support from an Ohio State Presidential Fellowship awarded to JRL and a grant from the Ohio Water Development Authority to fund the treatment sequences. FT-ICR-MS measurements were performed on the Bruker 15T FT-ICR housed by the Ohio State Mass Spectrometry and Proteomics facility, which was supported by the US National Institute of Health (S10 OD018507).

References

1 X. F. Li and W. A. Mitch, Drinking Water Disinfection Byproducts (DBPs) and Human Health Effects: Multidisciplinary Challenges and Opportunities, *Environ. Sci. Technol.*, 2018, **52**(4), 1681–1689, DOI: 10.1021/acs.est.7b05440.
2 S. D. Richardson and C. Postigo, Formation of DBPs: State of the Science, in *Recent Advances in Disinfection By-Products*, ed. T. Karanfil, American Chemical Society, 2015.
3 S. D. Richardson and M. J. Plewa, To regulate or not to regulate? What to do with more toxic disinfection by-products?, *J. Environ. Chem. Eng.*, 2020, **8**(4), 103939, DOI: 10.1016/j.jece.2020.103939.
4 M. J. Plewa and S. D. Richardson, Disinfection By-Products in Drinking Water, Recycled Water and Wastewater:

Formation, Detection, Toxicity and Health Effects: Preface, *J. Environ. Sci.*, 2017, **58**, 1, DOI: 10.1016/j.jes.2017.07.017.

5 U. E. P. Agency, National primary drinking water regulations: Stage 2 disinfectants and disinfection byproducts rule 71 FR 387, 2006.

6 S. Chowdhury, P. Champagne and P. J. McLellan, Models for predicting disinfection byproduct (DBP) formation in drinking waters: a chronological review, *Sci. Total Environ.*, 2009, **407**(14), 4189–4206, DOI: 10.1016/j.scitotenv.2009.04.006.

7 G. Hua, D. A. Reckhow and I. Abusallout, Correlation between SUVA and DBP formation during chlorination and chloramination of NOM fractions from different sources, *Chemosphere*, 2015, **130**, 82–89, DOI: 10.1016/j.chemosphere.2015.03.039.

8 T. Bond, E. H. Goslan, S. A. Parsons and B. Jefferson, A critical review of trihalomethane and haloacetic acid formation from natural organic matter surrogates, *Environ. Technol. Rev.*, 2012, **1**(1), 93–113, DOI: 10.1080/09593330.2012.705895.

9 A. D. Shah and W. A. Mitch, Halonitroalkanes, halonitriles, haloamides, and N-nitrosamines: a critical review of nitrogenous disinfection byproduct formation pathways, *Environ. Sci. Technol.*, 2012, **46**(1), 119–131, DOI: 10.1021/es203312s.

10 E. D. Wagner and M. J. Plewa, CHO cell cytotoxicity and genotoxicity analyses of disinfection by-products: An updated review, *J. Environ. Sci.*, 2017, **58**, 64–76, DOI: 10.1016/j.jes.2017.04.021.

11 T. Bond, J. Huang, M. R. Templeton and N. Graham, Occurrence and control of nitrogenous disinfection by-products in drinking water–a review, *Water Res.*, 2011, **45**(15), 4341–4354, DOI: 10.1016/j.watres.2011.05.034.

12 P. Westerhoff and H. Mash, Dissolved organic nitrogen in drinking water supplies: a review, *J. Water Supply: Res. Technol.–AQUA*, 2002, **51**(8), 415–448.

13 D. Wang, J. Xie, C. W. K. Chow, L. Xing and J. van Leeuwen, Characterization and predicting DOM treatability by enhanced coagulation, *Water Sci. Technol.: Water Supply*, 2012, **13**(1), 147, DOI: 10.2166/ws.2012.095.

14 M. Sillanpaa, M. C. Ncibi, A. Matilainen and M. Vepsalainen, Removal of natural organic matter in drinking water treatment by coagulation: A comprehensive review, *Chemosphere*, 2018, **190**, 54–71, DOI: 10.1016/j.chemosphere.2017.09.113.

15 A. Matilainen, N. Lindqvist and T. Tuhkanen, Comparison of the efficiency of aluminium and ferric sulphate in the removal of natural organic matter during drinking water treatment process, *Environ. Sci. Technol.*, 2005, **26**, 867–876.

16 H. C. Kim and M. J. Yu, Characterization of natural organic matter in conventional water treatment processes for selection of treatment processes focused on DBPs control, *Water Res.*, 2005, **39**(19), 4779–4789, DOI: 10.1016/j.watres.2005.09.021.

17 F. Wang, B. Gao, Q. Yue, F. Bu and X. Shen, Effects of ozonation, powdered activated carbon adsorption, and coagulation on the removal of disinfection by-product precursors in reservoir water, *Environ. Sci. Pollut. Res.*, 2017, **24**(21), 17945–17954, DOI: 10.1007/s11356-017-9451-1.

18 K. K. Shimabuku, A. M. Kennedy, R. E. Mulhern and R. S. Summers, Evaluating Activated Carbon Adsorption of Dissolved Organic Matter and Micropollutants Using Fluorescence Spectroscopy, *Environ. Sci. Technol.*, 2017, **51**(5), 2676–2684, DOI: 10.1021/acs.est.6b04911.

19 Y. Zhang, W. Chu, D. Yao and D. Yin, Control of aliphatic halogenated DBP precursors with multiple drinking water treatment processes: Formation potential and integrated toxicity, *J. Environ. Sci.*, 2017, **58**, 322–330, DOI: 10.1016/j.jes.2017.03.028.

20 G. Amy, L. Tan and M. K. Davis, The Effects of Ozonation and Activated Carbon Adsorption on Trihalomethane Speciation, *Water Res.*, 1991, **25**(2), 191–202.

21 A. A. Cuthbertson, S. Y. Kimura, H. K. Liberatore, D. R. U. Knappe, B. Stanford, R. S. Summers, E. R. Dickenson, J. C. Maness, C. Glover and M. Selbes, *et al.*, GAC to BAC: Does it make chloraminated drinking water safer?, *Water Res.*, 2020, **172**, 115432, DOI: 10.1016/j.watres.2019.115432, From NLM Medline.

22 A. A. Cuthbertson, S. Y. Kimura, H. K. Liberatore, R. S. Summers, D. R. U. Knappe, B. D. Stanford, J. C. Maness, R. E. Mulhern, M. Selbes and S. D. Richardson, Does Granular Activated Carbon with Chlorination Produce Safer Drinking Water? From Disinfection Byproducts and Total Organic Halogen to Calculated Toxicity, *Environ. Sci. Technol.*, 2019, **53**(10), 5987–5999, DOI: 10.1021/acs.est.9b00023.

23 P. C. Singer, J. H. Borchardt and J. M. Colthurst, The Effects of Permanganate Pretreatment on Trihalomethane Formation in Drinking Water, *J. - Am. Water Works Assoc.*, 1980, **72**(10), 573–578.

24 J. M. Colthurst and P. C. Singer, Removing trihalomethane precursors by permanganate oxidation and manganese dioxide adsorption, *J. - Am. Water Works Assoc.*, 1982, **74**(2), 78–83.

25 M. Chen, C. A. Rholl, S. L. Persaud, Z. Wang, Z. He and K. M. Parker, Permanganate preoxidation affects the formation of disinfection byproducts from algal organic matter, *Water Res.*, 2023, **232**, 119691, DOI: 10.1016/j.watres.2023.119691, From NLM Medline.

26 V. Rouge, U. von Gunten and S. Allard, Efficiency of pre-oxidation of natural organic matter for the mitigation of disinfection byproducts: Electron donating capacity and UV absorbance as surrogate parameters, *Water Res.*, 2020, **187**, 116418, DOI: 10.1016/j.watres.2020.116418, From NLM Medline.

27 J. Hu, W. Chu, M. Sui, B. Xu, N. Gao and S. Ding, Comparison of drinking water treatment processes combinations for the minimization of subsequent disinfection by-products formation during chlorination and chloramination, *Chem. Eng. J.*, 2018, **335**, 352–361, DOI: 10.1016/j.cej.2017.10.144.

28 J. R. Laszakovits, A. Kerr and A. A. MacKay, Permanganate Oxidation of Organic Contaminants and Model Compounds,

Environ. Sci. Technol., 2022, **56**(8), 4728–4748, DOI: 10.1021/acs.est.1c03621.

29 J. R. Laszakovits and A. A. MacKay, The impact of permanganate pre-oxidation on subsequent drinking water treatment operations, *Aquat. Sci.*, 2023, **85**(1), 33, DOI: 10.1007/s00027-022-00916-w.

30 T. Dittmar, B. Koch, N. Hertkorn and G. Kattner, A simple and efficient method for the solid-phase extraction of dissolved organic matter (SPE-DOM) from seawater, *Limnol. Oceanogr.:Methods*, 2008, **6**, 230–235.

31 B. Ballard and A. A. MacKay, Estimating the removal of anthropogenic organic chemicals from raw drinking water by coagulation-flocculation, *J. Environ. Eng.*, 2005, **131**, 108–118.

32 A. M. Kennedy and R. S. Summers, Effect of DOM Size on Organic Micropollutant Adsorption by GAC, *Environ. Sci. Technol.*, 2015, **49**(11), 6617–6624, DOI: 10.1021/acs.est.5b00411.

33 F. Zietzschmann, E. Worch, J. Altmann, A. S. Ruhl, A. Sperlich, F. Meinel and M. Jekel, Impact of EfOM size on competition in activated carbon adsorption of organic micro-pollutants from treated wastewater, *Water Res.*, 2014, **65**, 297–306, DOI: 10.1016/j.watres.2014.07.043.

34 K. Huang and A. D. Shah, Role of tertiary amines in enhancing trihalomethane and haloacetic acid formation during chlorination of aromatic compounds and a natural organic matter extract, *Environ. Sci.: Water Res. Technol.*, 2018, **4**(5), 663–679, DOI: 10.1039/c7ew00439g.

35 T. Chen, Spectrophotometric Determination of Microquantities of Chlorate, Chlorite, Hypochlorite, and Chloride in Perchlorate, *Anal. Chem.*, 1967, **39**(7), 804–813.

36 S. S. Lau, R. P. Dias, K. R. Martin-Culet, N. A. Race, M. H. Schammel, K. P. Reber, A. L. Roberts and J. D. Sivey, 1,3,5-Trimethoxybenzene (TMB) as a new quencher for preserving redox-labile disinfection byproducts and for quantifying free chlorine and free bromine, *Environ. Sci.: Water Res. Technol.*, 2018, **4**(7), 926–941, DOI: 10.1039/c8ew00062j.

37 C. M. Sharpless, M. Aeschbacher, S. E. Page, J. Wenk, M. Sander and K. McNeill, Photooxidation-Induced Changes in Optical, Electrochemical, and Photochemical Properties of Humic Substances, *Environ. Sci. Technol.*, 2014, **48**(5), 2688–2696, DOI: 10.1021/es403925g.

38 J. L. Weishaar, G. R. Aiken, B. A. Bergamaschi, M. S. Fram, R. Fujii and K. Mopper, Evaluation of specific ultraviolet absorption as an indicator of the chemical composition and reactivity of dissolved organic carbon, *Environ. Sci. Technol.*, 2003, **37**, 4702–4708, DOI: 10.1021/es030360x.

39 J. A. Korak and G. McKay, Critical review of fluorescence and absorbance measurements as surrogates for the molecular weight and aromaticity of dissolved organic matter, *Environ. Sci.: Processes Impacts*, 2024, **26**(10), 1663–1702, DOI: 10.1039/d4em00183d, From NLM Medline.

40 A. D. Zaffiro, M. Zimmerman, B. V. Pepich, R. W. Slingsby, R. F. Jack, C. A. Pohl and D. J. Munch, Method 557: Determination Of Haloacetic Acids, Bromate, And Dalapon In Drinking Water By Ion Chromatography Electrospray Ionization Tandem Mass Spectrometry (IC-ESI-MS/MS), 2009.

41 J. W. Hodgeson, A. L. Cohen, D. J. Munch and D. P. Hautman, Method 551.1: Determination of chlorination disinfection byproducts, chlorinated solvents, and halogenated pesticides/herbicides in drinking water by liquid-liquid extraction and gas chromatography with electron capture detection.

42 J. W. Munch and M. V. Bassett Method 521: Determination Of Nitrosamines In Drinking Water By Solid Phase Extraction And Capillary Column Gas Chromatography With Large Volume Injection And Chemical Ionization Tandem Mass Spectrometry (MS/MS), 2004.

43 T. Zeng, C. M. Glover, E. J. Marti, G. C. Woods-Chabane, T. Karanfil, W. A. Mitch and E. R. Dickenson, Relative Importance of Different Water Categories as Sources of N-Nitrosamine Precursors, *Environ. Sci. Technol.*, 2016, **50**(24), 13239–13248, DOI: 10.1021/acs.est.6b04650.

44 S. W. Krasner, W. A. Mitch, D. L. McCurry, D. Hanigan and P. Westerhoff, Formation, precursors, control, and occurrence of nitrosamines in drinking water: a review, *Water Res.*, 2013, **47**(13), 4433–4450, DOI: 10.1016/j.watres.2013.04.050.

45 W. A. Mitch, S. W. Krasner, P. Westerhoff and A. Dotson, *Occurrence and Formation of Nitrogenous Disinfection By-Products*, 2009.

46 J. R. Laszakovits, A. Somogyi and A. A. MacKay, Chemical Alterations of Dissolved Organic Matter by Permanganate Oxidation, *Environ. Sci. Technol.*, 2020, **54**(6), 3256–3266, DOI: 10.1021/acs.est.9b06675.

47 J. H. Gross, *Mass Spectrometry: A Textbook*, Springer, 2011.

48 J. Pei, C.-C. Hsu, Y. Wang and K. Yu, Corona discharge-induced reduction of quinones in negative electrospray ionization mass spectrometry, *RSC Adv.*, 2017, **7**(69), 43540–43545, DOI: 10.1039/c7ra08523k.

49 R. Vessecchi, Z. Naal, J. N. Lopes, S. E. Galembeck and N. P. Lopes, Generation of naphthoquinone radical anions by electrospray ionization: solution, gas-phase, and computational chemistry studies, *J. Phys. Chem. A*, 2011, **115**(21), 5453–5460, DOI: 10.1021/jp202322n, From NLM Medline.

50 J. Pei, C. C. Hsu, R. Zhang, Y. Wang, K. Yu and G. Huang, Unexpected Reduction of Iminoquinone and Quinone Derivatives in Positive Electrospray Ionization Mass Spectrometry and Possible Mechanism Exploration, *J. Am. Soc. Mass Spectrom.*, 2017, **28**(11), 2454–2461, DOI: 10.1007/s13361-017-1770-4, From NLM PubMed-not-MEDLINE.

51 G. J. Van Berkel, S. A. McLuckey and G. L. Glish, Electrochemical origin of radical cations observed in electrospray ionization mass spectra, *Anal. Chem.*, 1992, **64**(14), 1586–1593, DOI: 10.1021/ac00038a015.

52 A. Kruve, K. Kaupmees, J. Liigand, M. Oss and I. Leito, Sodium adduct formation efficiency in ESI source, *J. Mass Spectrom.*, 2013, **48**(6), 695–702, DOI: 10.1002/jms.3218.

53 A. Kruve and K. Kaupmees, Adduct Formation in ESI/MS by Mobile Phase Additives, *J. Am. Soc. Mass Spectrom.*, 2017, **28**(5), 887–894, DOI: 10.1007/s13361-017-1626-y.

54 G. R. Famini, B. C. Marquez and L. Y. Wilson, Using Theoretical Descriptors in Quantitative Structure-Activity Relationships: Gas Phase Acidity, *J. Chem. Soc., Perkin Trans. 1*, 1993, **2**, 773–782.

